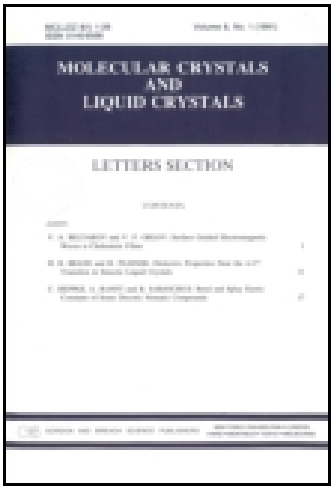

Molecular Crystals and Liquid Crystals
Publication details, including instructions for authors and subscription information:
http://www.tandfonline.com/loi/gmcl20

Properties of Bulk Heterojunction Organic Solar Cells with LiF Buffer Layer at Various Concentrations of Active Layer

Byung Min Park[a] & Ho Jung Chang[a]
[a] Department of Electronics Engineering, Dankook University, Cheonan-si, Chungnam, Korea
Published online: 06 Dec 2014.

To cite this article: Byung Min Park & Ho Jung Chang (2014) Properties of Bulk Heterojunction Organic Solar Cells with LiF Buffer Layer at Various Concentrations of Active Layer, Molecular Crystals and Liquid Crystals, 602:1, 177-184, DOI: 10.1080/15421406.2014.944760

To link to this article: http://dx.doi.org/10.1080/15421406.2014.944760

Mol. Cryst. Liq. Cryst., Vol. 602: pp. 177–184, 2014

ISSN: 1542-1406 print/1563-5287 online
DOI: 10.1080/15421406.2014.944760

Taylor & Francis
Taylor & Francis Group

Properties of Bulk Heterojunction Organic Solar Cells with LiF Buffer Layer at Various Concentrations of Active Layer

BYUNG MIN PARK AND HO JUNG CHANG*

Department of Electronics Engineering, Dankook University, Cheonan-si, Chungnam, Korea

*We fabricated organic solar cells (OSCs) using poly[2,6(4,4'bis(ethylhexyl)dithieno [3,2-b:2′,3′-*d*]silole)-alt-(1,3-(5-octyl-4H-thieno[3,4-*c*]pyrrole-4,6(5H)-dione))] (PDTSTPD) and (6,6)-phenyl-C_{71} butyric acid methyl ester ($PC_{71}BM$) active materials. PDTSTPD and $PC_{71}BM$ solutions for the active layer were mixed at concentration ratios of 1:1, 1:2, 1:3, and 1:4 wt%, respectively. The effects of OSCs at various concentrations of active layer on the electrical and morphological properties of the device were investigated. The performance of the OSC at a concentration ratio of 1:3 wt% showed the best electrical properties among the prepared samples, indicating that the maximum short circuit current density (J_{sc}), open circuit voltage (V_{oc}) and power conversion efficiency (PCE) values were about 6.9 mA/cm^2, 0.849 V and 2.3%, respectively. PDTSTPD:$PC_{71}BM$ active layer with a concentration ratio of 1:3 wt% showed smooth film roughness compared to the other prepared samples, which may lead to an improvement of the electron injection efficiency into the cathode electrode.*

Keywords Organic solar cell; LiF; PDTSTPD; $PC_{71}BM$; concentration ratio; power conversion efficiency

Introduction

Polymer fullerene-based bulk heterojunction (BHJ) organic solar cells (OSCs) have been considered highly promising candidates for photovoltaic devices because of their good features such as simple fabrication process, low cost, light weight, and flexible large-area applications [1–4]. In addition, the band gap of the organic materials can be easily tuned chemically by the incorporation of various functional elements. However, the low efficiency and poor stability of the OSCs compared with silicon-based solar cells, limits their feasibility for commercial use. For future commercial applications, it would be necessary to increase the power conversion efficiency (PCE) through the introduction of new active materials and the optimization of the manufacturing process [5–7]. Larger PCE values have been achieved by introducing the BHJ concept to replace the bi-layer structure of OSCs [5, 8]. The BHJ structure provides not only high surface contacts for the charge separation,

*Address correspondence to Prof. Ho Jung Chang, Department of Electronics Engineering, Dankook University, San 29, Anseo-dong, Dongnam-gu, Cheonan-si, Chungnam, 330-714, Korea (ROK). E-mail: hjchang@dankook.ac.kr

Color versions of one or more of the figures in the article can be found online at www.tandfonline.com/gmcl.

but also an interpenetrating network that enables efficient charge transportation [9]. Until now, the PCE values of these BHJ OSCs have reached as high as 7-9% [10–12]. Although the PCE values of OSCs have generally been low, various fabrication methods have been demonstrated for building an organic based active layer, such as spin-coating [13, 14], inkjet printing [15, 16], spray-coating [17, 18], and screen printing [19, 20]. Recently, in order to improve the PCE value, researchers have been trying to optimize the process conditions of OSCs. In particular, modification of the interface between the polymer active layer and the electrode film has been comprehensively carried out for improvement of the low charge injection and collection, especially due to mismatched energy levels between polymer materials and metal electrodes [21, 22]. In order to modify the interface between the active layer and an aluminum (Al) cathode film, lithium fluoride (LiF) film was introduced into OSC devices as a buffer layer in a previous study, where we reported the dependence of the LiF buffer layers on the electrical and optical properties of the OSC devices using Poly(3-hexylthiophene-2,5-diyl) (P3HT) and (6,6)-phenyl-C_{61}-butyric acid methyl ester ($PC_{61}BM$) active layers [23].

In this study, we prepared BHJ structure OSCs using poly[2,6(4,4′bis(ethylhexyl)dithieno[3,2-b:2′,3′-*d*]silole)-alt-(1,3-(5-octyl-4H-thieno[3,4-*c*]pyrrole-4,6(5H)-dione))] (PDTSTPD) and (6,6)-phenyl-C_{71} butyric acid methyl ester ($PC_{71}BM$) active materials. The effects of the concentration ratios of the active layer on the electrical and optical properties of the OSC devices with the LiF buffer layer were investigated, and we compared them to find out the optimum concentration ratio.

Experimental

Figure 1 shows (a) the energy band diagram related to the work functions of the OSC, (b) a schematic drawing of the device structure with the LiF cathode buffer layer, and (c) the chemical structures of the poly(3,4-ethylenedioxythiophene):poly(styrenesulfolnate) (PEDOT:PSS) hole transport materials as well as the PDTSTPD (Lumtec) [24] and $PC_{71}BM$ (Nano-c) [25] as an electrical donor and acceptor materials. In order to fabricate the OSCs, patterned indium tin oxide (ITO)-coated glass substrates with a sheet resistance of 15 Ω/square were cleaned with acetone, methanol and isoprophyl alcohol for 5 minutes in an ultrasonic bath. After the cleaning process, the substrate was dried and treated with UV-ozone for 15 minutes. UV-ozone treatment was carried out in order to improve the adhesion between the ITO electrode and the organic film layer. The PEDOT:PSS (CLEVIOS™ P VP AI 4083) was filtered with a 0.45-μm polyvinylidiene fluoride (PVDF) membrane filter. Then, the PEDOT:PSS solution was deposited directly onto an ITO/glass substrate by spin-coating method and baked at 140°C for 10 minutes on a hot plate. For the preparation of the PDTSTPD and $PC_{71}BM$ precursor solutions, PDTSTPD and $PC_{71}BM$ powders were combined and dissolved with various concentration ratios of 1:1, 1:2, 1:3, and 1:4 wt% using 1,2-dichlorobenzene on a hot plate at 60°C for 12 hours. The prepared PDTSTPD:$PC_{71}BM$ solution was spin-coated at 500 rpm for 60 seconds. And then, PDTSTPD:$PC_{71}BM$ film was annealed at 150°C for 10 minutes on a hot plate. The film thicknesses of the PEDOT:PSS and the PDTSTPD:$PC_{71}BM$ active layers were found to be about 40 and 100 nm, respectively. Following the spin-coating process of the active layer, LiF/Al cathode bi-layer films were deposited using a thermal evaporation method under high vacuum conditions of 5×10^{-7} Torr, in which the evaporation rates were about 1 and 2 Å/sec for the LiF and the Al electrode. The thicknesses were 0.5 and 150 nm for the LiF and Al, respectively. The active area of the OSC device was about 0.08 cm^2, which was defined by a shadow mask. The fabrication process of the OSC devices is shown in Fig. 2.

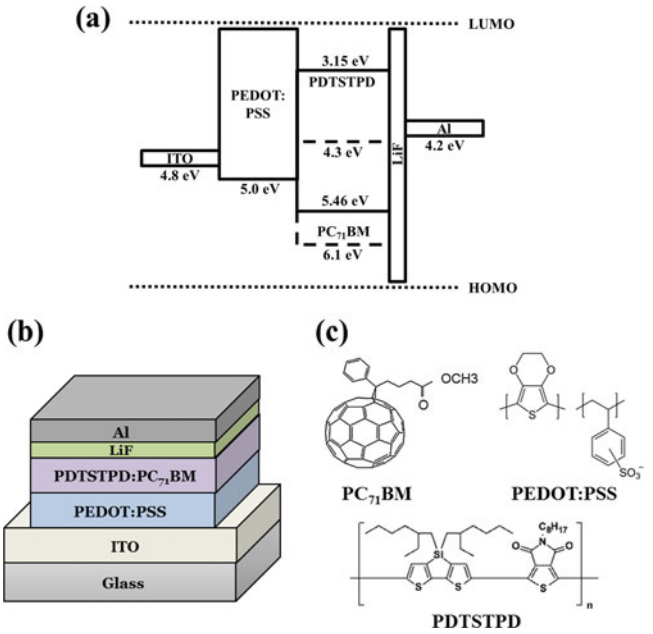

Figure 1. (a) Energy band diagram of the OSC devices, (b) schematic drawing of the device structures with the LiF cathode buffer layers and (c) chemical structures of the PEDOT:PSS, PDTSTPD and $PC_{71}BM$ organic materials for OSC devices.

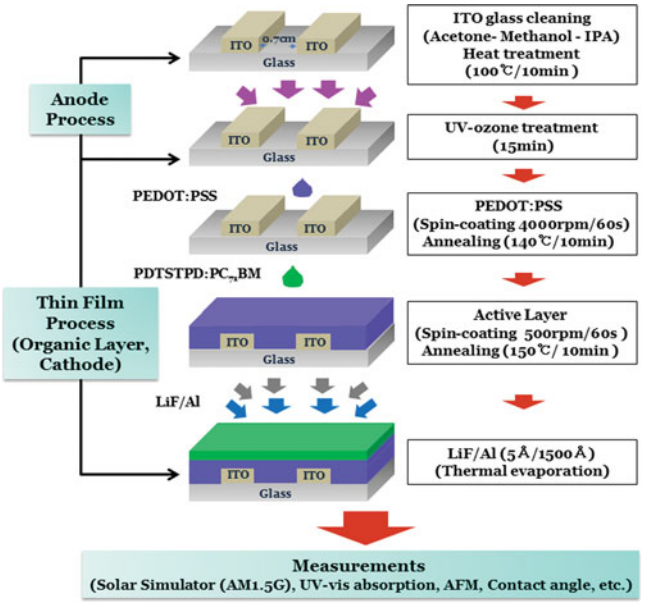

Figure 2. Fabrication process of the OSC devices.

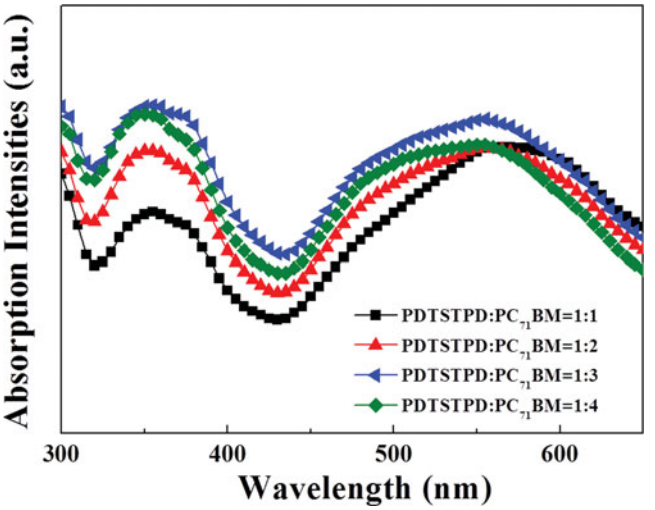

Figure 3. Light absorption spectra of the PDTSTPD:$PC_{71}BM$ active layers coated on PEDOT:PSS/ITO/glass substrates at various concentration ratios of 1:1, 1:2, 1:3, and 1:4 wt%.

The ultraviolet-visible (UV-vis) absorption spectra and the transmittance of films on ITO substrates were measured by a UV-vis spectrophotometer (MECASYS Optizen 2120UV). The current density-voltage (*J*-*V*) characteristics of devices under dark and illumination (AM 1.5G, 100 mW/cm^2) were determined by a Keithley 2400 source-meter at room temperature in air. The light intensity for the solar simulator (Oriel instruments with 150W Xenon lamp) was calibrated with a standard photovoltaic reference cell (Oriel reference solar cell). Atomic force microscopy (AFM) images were obtained by a scanning probe microscope (Bruker Innova-IRIS) operated in tapping mode. The AFM was used to investigate the surface morphology of the film layers with calculated root-mean-square (RMS) surface roughness values.

Results and Discussion

Figure 3 shows the intensities of the light absorption spectra of the PDTSTPD:$PC_{71}BM$ active layers coated on PEDOT:PSS/ITO/glass at various concentration ratios of 1:1, 1:2, 1:3 and 1:4 wt%. It was observed that the PDTSTPD:$PC_{71}BM$ active layer prepared from the concentration ratio of 1:3 wt% showed higher light absorption intensities on the whole at the wavelength range of around 320 to 550 nm, compared to other samples. This result shows that the optical properties of the active layer are affected by the $PC_{71}BM$ concentration ratio, suggesting that a large number of photons can be absorbed in the PDTSTPD:$PC_{71}BM$ active layer with the concentration ratio of 1:3 wt%. It is expected that the high light absorption intensity could lead to an improvement of the charge separation efficiency and the dissociated carrier mobility.

In this experiment, we found that the tendency of the light absorptions for the prepared devices was changed according to the measured wavelength ranges, indicating that the absorption intensities of the samples with the concentration ratios of PDTSTPD:$PC_{71}BM$ = 1:3 and 1:4 wt% were stronger rather than the one with the concentration ratio of PDTSTPD:$PC_{71}BM$ = 1:2 wt% in the wavelength range between 300 and 550 nm. In contrast, the light absorption intensity was reversed in the wavelength range above 550

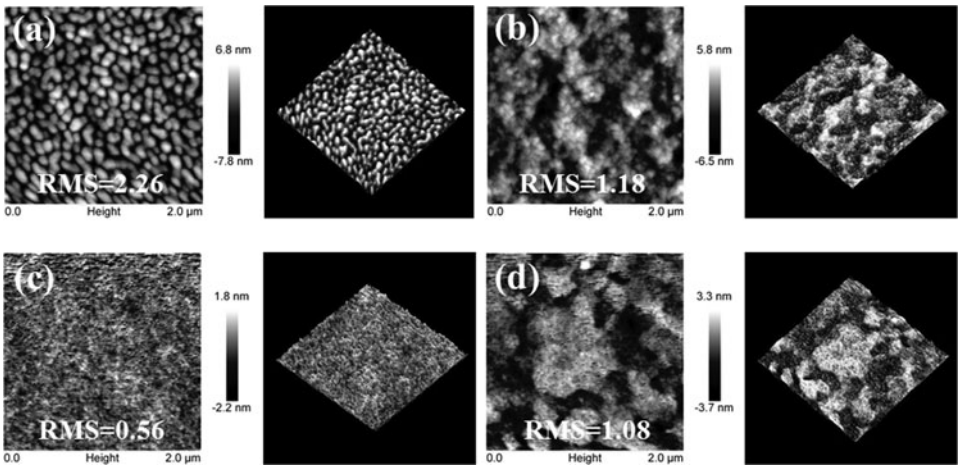

Figure 4. AFM surface morphologies and RMS values of the PDTSTPD:PC_{71}BM active film layers with various concentration ratios.

nm, showing the lowest optical absorption intensity was the sample with PDTSTPD:PC_{71}BM = 1:4 wt%.

The surface morphologies of the PDTSTPD:PC_{71}BM active layer may affect the performance of the OSC devices. Therefore, we studied the dependence of the surface morphologies and roughness of the PDTSTPD:PC_{71}BM active layers at various concentration ratios on the electrical and optical properties of the devices.

Figure 4 shows the AFM surface morphologies and RMS value of the PDTSTPD:PC_{71}BM active layers at various concentration ratios. The RMS values of the active layers with the concentration ratios of 1:1, 1:2, 1:3, and 1:4 wt% were found to be 2.26, 1.18, 0.56, and 1.08 nm, respectively. The RMS value decreased greatly from 2.26

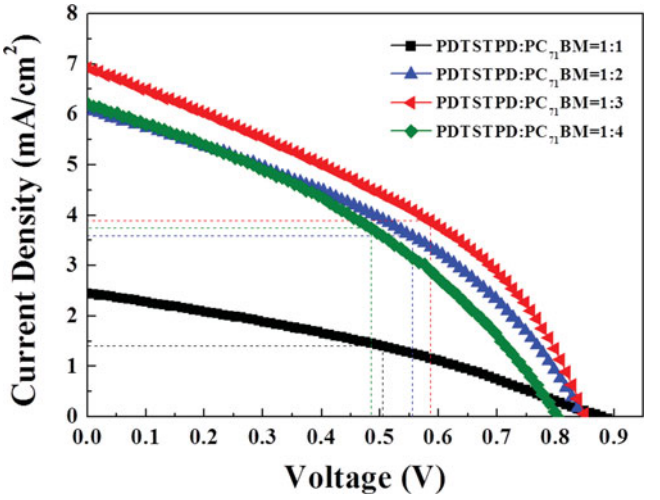

Figure 5. Current density versus voltage characteristic curves of the OSCs with PDTSTPD:PC_{71}BM active layer prepared from various concentration ratios of 1:1, 1:2, 1:3, and 1:4 wt%.

Table 1. The photovoltaic parameters (V_{oc}, J_{sc}, FF, PCE, R_s values) of the prepared OSCs with the LiF buffer layer at different concentration ratios of the PDTSTPD:$PC_{71}BM$ active layer

Samples (PDTSTPD:$PC_{71}BM$)	V_{OC} (V)	J_{SC} (mA/cm^2)	FF (%)	PCE (%)	R_S (**k**Ωcm^2)
1:1 wt%	0.879	2.5	32.9	0.7	3.24
1:2 wt%	0.849	6.1	38.2	2.0	0.57
1:3 wt%	0.849	6.9	38.7	2.3	0.41
1:4 wt%	0.808	6.2	36.2	1.8	0.72

to 0.56 nm as the PDTSTPD:$PC_{71}BM$ concentration was increased from 1:1 to 1:3 wt%, indicating smooth film surfaces at higher doping concentrations of the $PC_{71}BM$ electron acceptor material. These results may be related to the dense film formation when the precursor solution is spin-coated at the higher $PC_{71}BM$ concentrations, as shown in the surface morphology photographs. The rough film surface of the active layer may be caused by poor interfacial adhesion between the active layer and cathode film, resulting in a low injection efficiency of the carriers (holes) [26].

Figure 5 shows the current density versus voltage (*J-V*) characteristic curves and device parameters of the J_{sc}, V_{oc}, FF and PCE values of the OSCs with PDTSTPD:$PC_{71}BM$ active layers prepared with various concentration ratios. The maximum J_{sc} and FF values for the sample with the concentration ratio of 1:3 wt% were found to be 6.9 mA/cm^2 and 38.7%, respectively, indicating that the PCE was calculated to be 2.3%. From our experiments, it may be concluded that the observed improvement in the electrical and optical properties of the OSCs with the active layer concentration ratio of 1:3 wt% originated from the enhanced light absorption and smooth film surface due to the optimized concentration and dense film formation of the active layer. In addition, the increased J_{sc} value reflects the improved exporting efficiency of the carriers into electrodes. When the exciton (electrons and holes) quenching phenomenon occurs in the active layer, the electrical property is deteriorated in the device at a certain $PC_{71}BM$ concentration [27]. Therefore, according to the results of *J-V* characteristics, the exciton quenching was likely to have occurred for the samples with the maximum concentration ratio of 1:4 wt% in the active layer.

For an ideal photovoltaic device, a low series resistance (R_s) is required [28]. R_s can be expressed as the sum of the bulk resistance and contact resistance. The FF value is correlated with R_s, J_{sc}, and V_{oc}, as formulated in Eq. (1) [29]:

$$FF = FF_0 \left[1 - R_s \left(J_{sc}\right)\right] / V_{oc} \tag{1}$$

where FF_0 is the ideal characteristic of the device. The R_s originates from the Ohmic loss in the OSC device.

The R_s value for the sample with the 1:3 wt% concentration ratio of PDTSTPD: $PC_{71}BM$ in the active layer was about 0.41 kΩ cm^2, which is the lowest value among the prepared samples. The low R_s of the device is responsible for the increase of the J_{sc}, due to the formation of a better Ohmic contact. Generally, V_{oc} is strongly dependent on the differences of the energy level between highest occupied molecular orbit of the donor (PDTSTPD) and lowest unoccupied molecular orbit of acceptor ($PC_{71}BM$) materials. In this experiment, V_{oc} changed greatly as the concentration ratio of PDTSTPD:$PC_{71}BM$

active materials increased from 1:1 to of 1:4 wt%. Therefore, it would be necessary to carry out the further experiments for the actual energy levels of the PDTSTPD:$PC_{71}BM$ active materials with different concentration ratios.

The J_{sc}, V_{oc}, FF, PCE, and R_s values of the prepared OSCs with the LiF buffer layer at different concentration ratios of the PDTSTPD:$PC_{71}BM$ active layer are summarized in Table 1.

Conclusions

Organic solar cells (OSCs) using PDTSTPD and $PC_{71}BM$ in the active layer as the electron donor and acceptor materials were manufactured by the spin-coating method. OSCs with the structure of glass/ITO/PEDOT:PSS/PDTSTPD:$PC_{71}BM$/LiF/Al were prepared and investigated regarding the effects of the concentration ratios of the active layer on the properties of the OSC devices. As a result, the optical, morphological, and electrical properties of the PDTSTPD:$PC_{71}BM$ active layer were affected by the concentration ratios of the active materials. The performance of the OSC device with a 1:3 wt% concentration ratio of the active materials was superior to the other prepared samples, showing maximum J_{sc}, V_{oc}, FF, and PCE values of about 6.9 mA/cm^2, 0.849 V, 38.7% and 2.3%, respectively. According to the AFM morphologies and light absorption spectra of the active film layers, the improved electrical properties may be attributable to a smooth film surface and higher light absorption intensity of the active layer.

Funding

This work was supported by the National Research Foundation of Korea (NRF) grant funded by the Korea government (MEST : 2011-0015835).

References

[1] Yu, G., Gao, J., Hummelen, J. C., Wudl, F., & Heeger, A. J. (1995). *Science*, *270*, 1789.
[2] Krebs, F. C. (2009). *Sol. Energy Mater. Sol. Cells*. *93*, 394.
[3] Cai, W., Gong, X., & Cao, Y. (2010). *Sol. Energy Mater. Sol. Cells*. *94*, 114.
[4] Zuo, L. J., Jiang, X. X., Xu, M. S., Yang, L. G., Nan, Y. X., Yan, Q. X., & Chen, H. Z. (2011). *Sol. Energy Mater. Sol. Cells. 95*, 2664.
[5] Tang, C. W. (1986). *Appl. Phys. Lett. 48*, 183.
[6] Karagiannidis, P.G., Kassavetis, S., Pitsalidis, C., & Logothetidis, S. (2011). *Thin Solid Films*, *519*, 4105.
[7] Ma, W., Yang, C., Gong, X., Lee, K., & Heeger, A. J. (2005). *Adv. Funct. Mater. 15*, 1617.
[8] Yu, G., & Heeger, A. J. (1995). *J. Appl. Phys. 78*, 4510.
[9] Kraabel, B., Hummelen, J. C., Vacar, D., Moses, D., Sariciftci, N. S., Heeger, A. J., & Wudl, F. (1996). *J. Chem. Phys. 104*, 4267.
[10] He, Z. C., Zhong, C. M., Huang, X., Wong, W. Y., Wu, H. B., Chen, L. W., Su, S. J., & Cao, Y. (2011). *Adv. Mater. 23*, 4636.
[11] Service, R. F. (2011). *Science*, *332*, 293.
[12] He, Z. C., Zhong, C. M., Su, S. J., Xu, M., Wu, H. B., & Cao, Y. (2012). *Nat. Photon. 6*, 591.
[13] Jang, S. K., Gong, S. C., & Chang, H. J. (2012). *Synth. Met. 162*, 426.
[14] Dennler, G., Scharber, M. C., & Brabec, C. J. (2009). *Adv. Mater. 21*, 1323.
[15] Aernouts, T., Aleksandrov, T., Girotto, C., Genoe, J., & Poortmans, J. (2008). *Appl. Phys. Lett. 92*, 033306–1.
[16] Teichler, A., Eckardt, R., Hoeppener, S., Friebe, C., Perelaer, J., Senes, A., Morana, M., & Brabec, C. J. (2011). *U.S. Schubert, Adv. Eng. Mater. 1*, 105.

[17] Susanna, G., Salamandra, L., Brown, T. M., Di Carlo, A., Brunetti, F., & Reale, A. (2011). *Sol. Energy Mater. Sol. Cells. 95*, 1775.
[18] Kang, J. W., Kang, Y. J., Jung, S., Song, M., Kim, D. G., Kim, C. S., & Kim, S. H. (2012). *Sol. Energy Mater. Sol. Cells. 103*, 76.
[19] Shaheen, S. E., Radspinner, R., Peyhambarian, N., & Jabbour, G. E. (2001). *Appl. Phys. Lett. 79*, 2996.
[20] Krebs, F. C., Jorgensen, M., Norrman, K., Hagemann, O., Alstrup, J., Nielsen, T. D., Fyenbo, J., Larsen, K., & Kristensen, J. (2009). *Sol. Energy Mater. Sol. Cells. 93*, 422.
[21] Yang, L. G., Chen, H. Z., & Wang, M. (2008). *Thin Solid Films*, *516*, 7701.
[22] Kim, K. J., Kim, Y. S., Kang, W. S., Kang, B. H., Yeom, S. H., Kim, D. E., Kim, J. H., & Kang, S. W. (2010). *Sol. Energy Mater. Sol. Cells. 94*, 1303.
[23] Kim, K. H., Gong, S. C., & Chang, H. J. (2012). *Thin Solid Films*, *521*, 69.
[24] Yuan, M. C., Chou, Y. J., Chen, C. M., Hsu, C. L., & Wei, K. H. (2011). *Polymer. 52*, 2792.
[25] Kim, J. Y., Lee, K., Coates, N. E., Moses, D., Nguyen, T. Q., Dante, M., & Heeger, A. J. (2007). *Science*, *317*, 222.
[26] Chen, H. Y., Hou, J., Zhang, S., Liang, Y., Yang, G., Yang, Y., Yu, L., Wu, Y., & Li, G. (2009). *Nat. Photon. 3*, 649.
[27] Chen, X., Zuo, L., Fu, W., Yan, Q., Fan, C., & Chen, H. (2013). *Sol. Energy Mater. Sol. Cells. 111*, 1.
[28] Xue, J., Uchida, S., Rand, B. P., & Forrest, S. R. (2004). *Appl. Phys. Lett. 84*, 3013.
[29] Mallajosyula, A. T., Srivastava, N., lyer, S. S. K., & Mazhari, B. (2010). *Sol. Energy Mater. Sol. Cells. 8*, 1319.